

MEASUREMENTS OF $B \rightarrow X_s \gamma$ AND STUDY OF $B \rightarrow X_s l^+ l^-$

G. EIGEN

*Department of Physics, University of Bergen, Allegaten 55, 5007 Bergen,
Norway*

E-mail: eigen@sfys2.fi.uib.no

The updated CLEO measurement of the electromagnetic penguin process $B \rightarrow X_s \gamma$ is presented and compared to the ALEPH result. Implications on new physics are discussed and the status of recent searches for $B \rightarrow X_s l^+ l^-$ modes is given.

1 Introduction

Flavor-changing neutral currents (FCNC) are forbidden in the Standard Model (SM) at tree level. They are, however, induced at higher orders via penguin processes or box diagrams. One such process is $B \rightarrow X_s \gamma$, which is mediated by electromagnetic (em) penguin loops. The lowest-order SM diagrams are shown in Figure 1. The dominant contribution arises from the magnetic dipole operator \mathcal{O}_7 . QCD corrections, however, cause mixing with the other operators \mathcal{O}_1 to \mathcal{O}_6 and \mathcal{O}_8 . The dominant short-distance effects are separated from the non-perturbative long-distance parts into perturbatively-calculable renormalization-scale-dependent Wilson coefficients. In $B \rightarrow X_s \gamma$ all perturbative contributions can be absorbed into a single effective function, $\tilde{C}_7^{eff}(\mu)$, which reduces to $C_7^{(0)eff}(5.0) = -0.300$ in leading-order QCD.¹ However, a 25% uncertainty in the decay rate arises from varying the renormalization scale between $m_b/2$ and $2m_b$. In next-to-leading order (NLO) calculated recently² this uncertainty is reduced by a factor 1.5-2.³

In the Standard Model the inclusive $B \rightarrow X_s \gamma$ decay rate is^{2,4}

$$\Gamma(B \rightarrow X_s \gamma) = \frac{m_b^5}{32\pi^4} G_F^2 \alpha_{em} |V_{tb} V_{ts}^*|^2 (|\tilde{C}_7^{eff}(\mu)|^2 + A), \quad (1)$$

where m_b , G_F , α_{em} , A , and $V_{tb} V_{ts}^*$ denote the b -quark mass, the Fermi constant, the em coupling constant, the bremsstrahlung contribution and Cabibbo-Kobayashi-Maskawa (CKM) matrix elements for $t \rightarrow b$ and $t \rightarrow s$ couplings, respectively. The $B \rightarrow X_s \gamma$ branching fraction is calculated by scaling the semileptonic decay rate, yielding $B(B \rightarrow X_s \gamma) = (3.28 \pm 0.33) \times 10^{-4}$ in NLO QCD.² Since the branching fraction is sensitive to additional contributions from *e.g.* a charged Higgs boson, a new gauge boson or a charged supersymmetric (SUSY) particle in the loop, $B \rightarrow X_s \gamma$ is well-suited to probe new physics. A branching fraction measurement *e.g.* can be used to constrain the SUSY

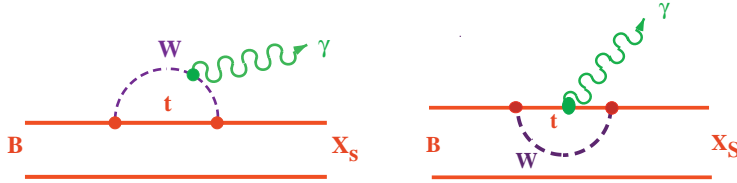


Figure 1: Lowest-order Feynman diagrams for $B \rightarrow X_s \gamma$ in the SM.

parameter space. CLEO was the first experiment to observe this process both in the exclusive $K^* \gamma$ final state⁵ and the inclusive channel.⁶

2 The recent CLEO $B \rightarrow X_s \gamma$ Measurement

The inclusive $B \rightarrow X_s \gamma$ analysis has been updated recently by CLEO using a sample of $3.3 \times 10^6 B\bar{B}$ pairs. The photon energy, which is nearly half the B mass ($\langle E_\gamma \rangle \simeq 2.4$ GeV), is the highest observed in any B decay. The Fermi motion of the b -quark inside the B mesons and the B meson momentum in the lab frame yield a Doppler-broadened photon line. According to spectator model predictions, 85% - 94% of the photons are in the $2.1 \text{ GeV} \leq E_\gamma \leq 2.7 \text{ GeV}$ energy range.⁷ While backgrounds from B decays are small, those from continuum processes, such as $e^+e^- \rightarrow q\bar{q}\gamma$ and $e^+e^- \rightarrow q\bar{q}$, are significant. To minimize these backgrounds an event shape analysis is combined with exclusive final-state reconstruction, considering only high-energy photons as candidates that are inconsistent with originating from a π^0 or η decay.

At the $\Upsilon(4S)$ the event shape of hadronic $B\bar{B}$ decays is spherical, while that of $q\bar{q}$ continuum is back-to-back. In $B \rightarrow X_s \gamma$ events the spherical symmetry is distorted by the hard photon. The event shape resembles more that of $q\bar{q}$ continuum with initial-state radiation (ISR). The ratio of second-to-zeroth Fox-Wolfram moments R_2 and the sphericity S_\perp are used to separate the signal from $q\bar{q}$ continuum. To suppress ISR continuum background 2 variables are evaluated in the rest frame of the e^+e^- following the radiation of a hard photon: the ratio of Fox Wolfram moments R'_2 , where the photon is excluded, and $\cos\theta'$, where θ' is the angle between the photon and the thrust axis of the rest of the event. In addition, the energy flow inside 20° and 30° cones parallel and antiparallel with the photon direction are calculated. With help of a neural network the 8 variables are combined into a single shape variable r_{sh} , which favors values of $r_{sh} \approx +1$ for $B \rightarrow X_s \gamma$ signal and $r_{sh} \approx -1$ for continuum background.

For additional suppression of continuum background the X_s system is reconstructed in exclusive final states. Considered are modes containing either a K^\pm or a $K_S^0 \rightarrow \pi^+\pi^-$ plus 1-4 π 's with at most one π^0 in addition to the hard photon. A global χ^2 based on the beam-constrained mass M_B , the energy difference ΔE , the dE/dx of the charged particles as well as the K_S^0 and π^0 masses is used for candidate selection. For the combination with the lowest χ^2 a second shape variable r_c is constructed using a neural network. The input variables are r_{sh} , the χ_B^2 value obtained from M_B and ΔE alone and $|\cos\theta_{tt}|$, where θ_{tt} is the angle between the thrust axes of the candidate B and the rest of the event. Again signal events peak at $r_c \approx +1$, while continuum background peaks at $r_c \approx -1$. Figures 2a,c show the r_c and r_{sh} distributions for signal and $q\bar{q}$ continuum obtained from Monte Carlo (MC).

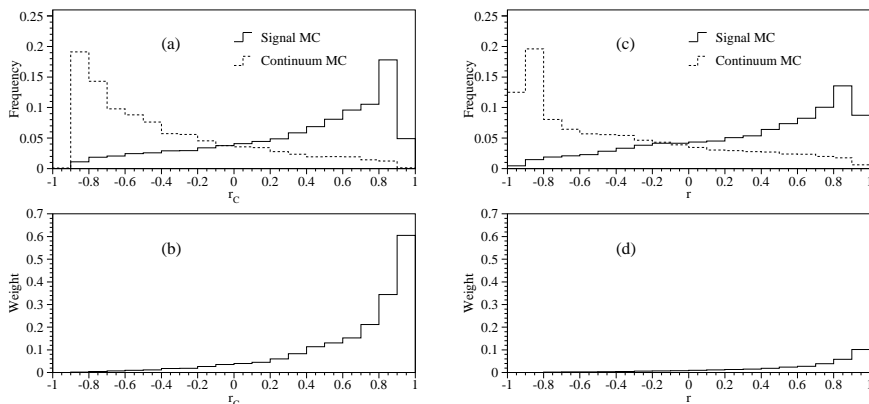


Figure 2: a) Distributions in the shape variable r_c for MC samples of $B \rightarrow X_s\gamma$ and $q\bar{q}$ continuum for events with $\chi_B^2 < 20$; b) event weighting function for r_c ; c) corresponding distributions in shape variable r_{sh} for events failing reconstruction; d) event weighting function for r_{sh} .

To optimize the signal-to-background ratio, the candidates are weighted by $w = s/[s + (1 + \alpha)b]$, where s and b are the expected signal and background yields for a given value of r_c and α is the luminosity scale factor between the $\Upsilon(4S)$ and the off-resonance data samples. Since just $\sim 20\%$ of signal events are exclusively reconstructed, a weighting based on r_{sh} alone is used for selected events which fail the exclusive reconstruction ($\chi_B^2 > 20$). The event weighting functions are displayed in Figures 2b,d.

Backgrounds from $B\bar{B}$ decays, where the photon originates from a π^0 or an

η decay, are estimated from Monte Carlo. However, the π^0 and η momentum spectra are adjusted to those observed in the data. The spectra are obtained by treating the π^0 or η like a photon, performing the same analysis as discussed above for photons using weights w . This procedure helps to account for inaccuracies in the $b \rightarrow cW^-$ and $b \rightarrow uW^-$ event generation and for omissions of modes such as $B \rightarrow X_s g$. Further analysis details are given in reference [9].

Figure 3a shows the weighted photon spectrum and the estimated contributions from $B\bar{B}$ and continuum backgrounds. The background-subtracted photon spectrum plotted in Figure 3b shows a clear signal in the 2.1-2.7 GeV region. The observed shape is consistent with the spectator model prediction.⁷ The weighted event yields in two bins below and one bin above the signal region are consistent with the background parametrization. The background-subtracted weighted event yield in the 2.1-2.7 GeV window amounts to $92.21 \pm 10.26_{stat} \pm 6.46_{sys}$ events. The systematic error consists of a $\pm 1\%$ uncertainty in the $q\bar{q}$ continuum subtraction and a 20% uncertainty in the $B\bar{B}$ subtraction, both added in quadrature.

The weighted efficiency in the 2.1-2.7 GeV is determined from the Ali-Greub model,⁷ which includes gluon bremsstrahlung and higher-order radiative effects. The Fermi momentum of the b -quark and the mass of the spectator quark are varied such that on average $\langle m_b \rangle = 4.88 \pm 0.1$ GeV. For the hadronization process both the JETSET algorithm⁸ and a mix of K^* resonances are used such that the X_s mass distribution predicted in the Ali-Greub model⁷ is reproduced. A weighted efficiency of $\epsilon_w = (4.70 \pm 0.23 \pm 0.23 \pm 0.04 \pm 0.33) \times 10^{-2}$ is determined in the signal region. The 4 errors represent uncertainties due to spectator model inputs, hadronization of the X_s system, the production ratio of B^+B^- and $B^0\bar{B}^0$ and detector modelling, respectively.

Combining the background-subtracted weighted event yield with the weighted efficiency results in a branching fraction of

$$B(B \rightarrow X_s \gamma) = (3.15 \pm 0.35_{stat} \pm 0.32_{sys} \pm 0.26_{model}) \times 10^{-4}. \quad (2)$$

This measurement is in good agreement with the Standard Model prediction. It supercedes the previous CLEO result, since 60% additional data are included and improved analysis techniques are used. The 95% confidence level (CL) limits including all systematic effects are

$$2.0 \times 10^{-4} < B(B \rightarrow X_s \gamma) < 4.5 \times 10^{-4}. \quad (3)$$

3 The $B \rightarrow X_s \gamma$ Result from ALEPH

At LEP the b and \bar{b} quark are separated into opposite hemispheres. The $B \rightarrow X_s \gamma$ hemisphere has low multiplicity, a single displaced vertex and a high-

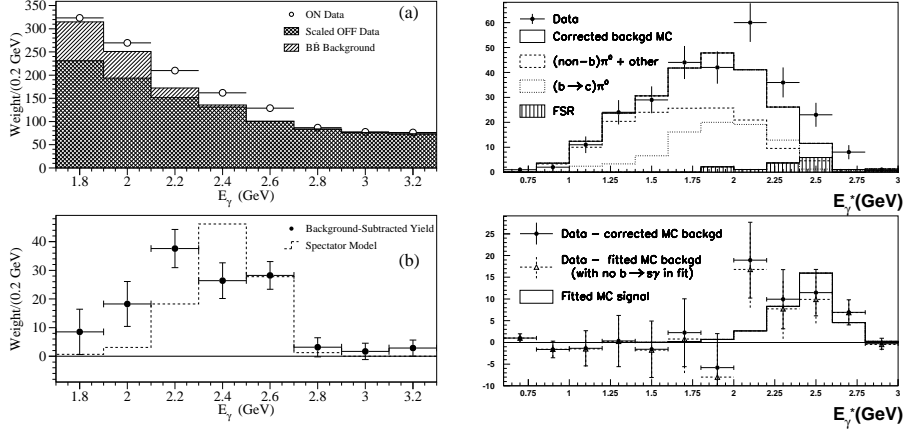


Figure 3: a) Observed weighted photon energy spectrum and background contributions from CLEO; b) background-subtracted photon yield and predicted shape of $B \rightarrow X_s \gamma$ signal.

Figure 4: top) Observed photon energy spectrum and background contributions from ALEPH; bottom) background-subtracted photon yield from multivariate fits.

energy photon, whereas the opposite hemisphere contains a typical b hadron decay that is used for a b -tagging. In a sample of $8.9 \times 10^5 b\bar{b}$ pairs, ALEPH selects $B \rightarrow X_s \gamma$ candidates with an inclusive reconstruction algorithm. First, probabilities P to originate from a $B \rightarrow X_s \gamma$ decay are defined for the candidate photon and the other particles (charged tracks, π^0 's, K_S^0 's and K_L^0 's) in the candidate jet, using rapidity, momentum and impact parameter. Second, the candidate photon and up to 8 particles in decreasing order of probability P are added until an invariant mass of the system closest to the B mass is obtained. In addition to standard b hadron selection criteria, the candidate photon has to be inconsistent with a π^0 decay; the $\gamma\gamma$ invariant mass when combined with another photon has to lie above 0.2 GeV. The photon energy has to exceed 10 GeV and θ_γ^* , the angle between the photon in the rest frame of the jet and the jet direction has to satisfy $\cos \theta_\gamma^* < 0.55$. While the signal is uniformly distributed, the background peaks at $\cos \theta_\gamma^* = +1$. The mass of the candidate B has to be within 0.7 GeV of the nominal B mass and the mass of the X_s system has to be below 4 GeV.

The resulting sample is divided into 8 subsamples, using the major axis of the electromagnetic shower ellipse σ_l to separate merged π^0 's from photons, the jet energy E_{jet} , and the probability P_{hem}^{opp} that all charged tracks in the opposite hemisphere are consistent with originating from the primary vertex. This

procedure provides an effective separation of signal photons from backgrounds that originate from π^0 's, final state radiation (FSR) and other sources. The signal is enhanced in the subsample with $E_{jet} > 32$ GeV, $\sigma_l < 2.3$ cm and $-\log P_{hem}^{opp} > 2.2$. The photon energy E_γ^* in the jet rest frame is plotted for this subsample in Figure 4. An excess is seen in the 2.2-2.8 GeV region. A binned log-likelihood fit is performed in all eight subsamples to extract the number of signal events and background events due to FSR, π^0 's from b decays, π^0 's from non- b decays and other sources. Of the 1560 candidates 69.4 ± 19.7 are found to be signal events. The largest backgrounds result from π^0 decays. The efficiency for selecting $B \rightarrow X_s \gamma$ signal is $\epsilon = 12.8 \pm 0.3\%$. Further details are discussed in the publication.¹⁰

From the yield in the 2.2-2.8 GeV energy interval one obtains an inclusive branching fraction of

$$B(B \rightarrow X_s \gamma) = (3.11 \pm 0.8 \pm 0.72) \times 10^{-4}. \quad (4)$$

This is in good agreement with the CLEO result and the SM prediction. The largest systematic error contributions are due to background shapes (0.462), background MC statistics (0.376), background MC composition (0.185), and energy calibration uncertainties (0.182).

4 Implications on New Physics

New physics processes can enhance the $B \rightarrow X_s \gamma$ decay rate. For example, in SUSY models one expects contributions from a charged Higgs and charginos in the loop as shown in Figure 5. These yield new contributions $C_7^{new}(M_W)$ and $C_8^{new}(M_W)$ to the SM Wilson coefficients at the M_W -scale. Due to operator mixing, $B \rightarrow X_s \gamma$ then limits the possible values for $C_i^{new}(M_W)$. To study the effect of $B \rightarrow X_s \gamma$ on SUSY, solutions in the SUSY parameter space have been generated using the minimal supergravity model (SUGRA).¹¹ The ranges of the input parameters are $0 < m_0 < 500$ GeV, $50 < m_{1/2} < 250$ GeV, $-3 < A_0/m_0 < 3$, $2 < \tan \beta < 50$ and $m_t = 175$ GeV.¹¹ Each solution is only kept if it is not in violation with present SLC/LEP constraints and Tevatron direct sparticle production limits. For these solutions the ratios $R_7 = C_7^{new}(M_W)/C_7^{SM}(M_W)$ and $R_8 = C_8^{new}(M_W)/C_8^{SM}(M_W)$ are calculated. The resulting scatter plot in the $R_7 - R_8$ plane is shown in Figure 6a. Many solutions are already in conflict with the present $B \rightarrow X_s \gamma$ measurement from CLEO (region inside solid bands).

To demonstrate the reach of $B \rightarrow X_s \gamma$ in probing SUSY in comparison to that of high-energy colliders, 5 points in the SUGRA model chosen at Snowmass 1996 for an NLC study are examined.¹² Point 3 is the common point for

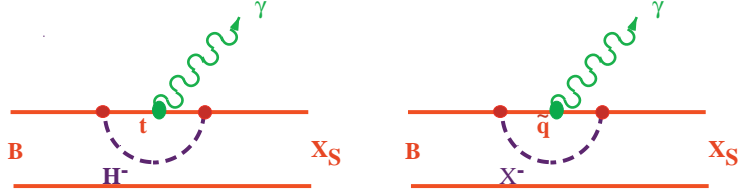


Figure 5: Feynman diagrams for new physics contribution to $B \rightarrow X_s \gamma$.

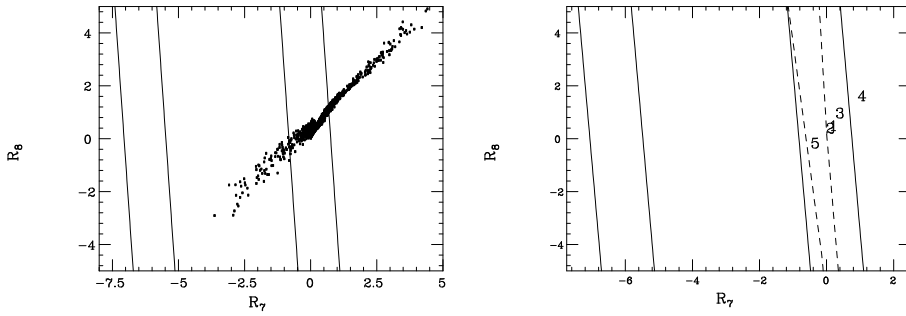


Figure 6: Scatter plot of R_8 vs R_7 for a) solutions in the SUGRA model and b) for 5 NLC SUGRA points. The allowed region from the CLEO measurement lies inside the 2 sets of solid diagonal bands. The dashed lines indicate a potential 10% measurement.

a comparison of SUSY studies at NLC, LHC and upgraded Tevatron. The sparticle mass spectra for these 5 points are obtained by SUGRA relations and their contribution to $B \rightarrow X_s \gamma$ can be computed. Figure 6b shows the results in the R_7 - R_8 plane.¹³ Also shown are the constraints obtained from fits to the present CLEO data (solid line) and a future 10% measurement assuming a SM value for the branching fraction (dashed line). While point 4 is already excluded by the present CLEO measurement, all but point 5 lie outside the dashed diagonal band. Thus, rare B decays provide a complementary approach to high-energy colliders in searching for SUSY.

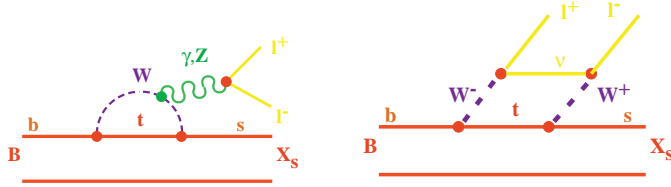


Figure 7: Lowest order Feynman diagrams for $B \rightarrow X_s l^+ l^-$ in SM.

5 Study of $B \rightarrow X_s l^+ l^-$ decays at CLEO

Another interesting and related process is $B \rightarrow X_s l^+ l^-$, where the photon is replaced with a lepton pair. The lowest-order SM diagrams are shown in Figure 7. In addition to the magnetic penguin operator \mathcal{O}_7 , the electroweak operators \mathcal{O}_9 and \mathcal{O}_{10} contribute, yielding 3 scale-dependent Wilson coefficients: $C_7(\mu)$, $C_9(\mu)$ and $C_{10}(\mu)$. Due to QCD effects, which are smaller here than in $B \rightarrow X_s \gamma$, again operator mixing occurs. Their contributions are absorbed into the effective Wilson coefficients $C_7^{(0)eff}(\mu)$ and $C_9^{eff}(\mu)$. The decay rate has been calculated in NLO. However, to maintain a scheme-independent result, only $C_9(\mu)$ is calculated in NLO while LO is retained for all other Wilson coefficients. New physics can affect any of these 3 Wilson coefficients. Due to the additional α_{em} coupling, the branching fractions predicted in SM are almost 2 orders of magnitude smaller than those for corresponding $B \rightarrow X_s \gamma$ modes.

Using a sample of 3.3×10^6 $B\bar{B}$ pairs CLEO has searched for both inclusive $X_s l^+ l^-$ channels and 8 exclusive final states, where a K or K^* recoils against $\mu^+ \mu^-$ or $e^+ e^-$. A detailed discussion of the inclusive analysis is given in reference [16]. In the exclusive analysis a Fisher discriminant method is used in addition to standard B selection criteria to suppress continuum background. It is constructed from the distributions of thrust and sphericity of the B candidate, the B direction in the lab frame and the angle between the thrust axes of the candidate B and the rest of the event. The candidate B is selected by a χ^2 method, which includes ΔE , the masses of intermediate resonances, and both the dE/dx and time-of-flight information of all charged tracks in the final state. The combination with the lowest χ^2 is retained. Since double semileptonic decays are a dominant background source, the missing energy of the event is constrained to $< 20\%$. To remove contributions from the color-suppressed $B \rightarrow \psi^{(\prime)} K^{(*)}$ modes, events with dilepton masses near the ψ and ψ' mass peaks are excluded. Signal regions are defined in the $M_B - \Delta E$

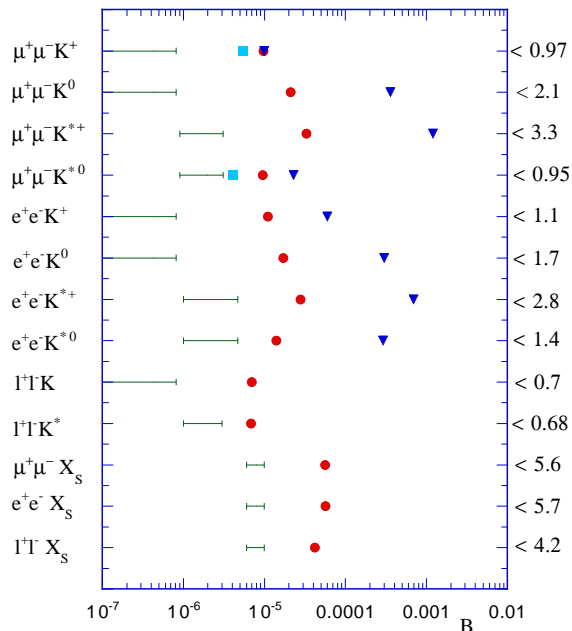


Figure 8: Branching fraction upper limits of $B \rightarrow X_s l^+ l^-$ modes at 90% CL from CLEO (solid points) in comparison to a range of SM predictions (solid lines), recent results from CDF (squares) and previous upper limits (triangles). The numbers on the right-hand side show the present CLEO limits in units of 10^{-5} .

plane by $\pm 2.5\sigma_M \times \pm 2.5\sigma_{\Delta E}$ wide boxes, where $\sigma_M, \sigma_{\Delta E}$ denote M_B and ΔE resolutions, respectively. Regions outside $3.5\sigma_M$ and $\sigma_{\Delta E}$ are used for background determination. No signal is observed in any of the 8 final states. The observed yields are consistent with expected backgrounds. The total efficiency is 4–5% for modes containing a K_S^0 or a K^{*+} , 8–10% for modes with a K^{*0} and 17–23% for modes with a K^+ . Further details are found in reference [17].

The resulting 90% CL upper limits are plotted in Figure 8 together with those of previous studies,¹⁸ recent CDF results¹⁹ and a range of SM predictions.³ The $K^{*0}l^+l^-$ upper limit has been set for $m_{l^+l^-} > 0.5$ GeV, to reduce the contribution from $C_7^{(0)eff}$. The new CDF and CLEO upper limits provide significant improvements, although they still lie above the SM predictions. The CDF upper limit closest to the SM prediction is that for $K^{*0}\mu^+\mu^-$ lying just a factor of 1.2 above. The most sensitive upper limit from CLEO is that for the combined $K^{*0}l^+l^-$ modes, which lies a factor of 2.2 above the SM predictions.

6 Conclusion

The present $B \rightarrow X_s \gamma$ measurement is in good agreement with the NLO SM prediction. The combined statistical and systematic errors are 15%, while the model dependence is 8%. Even with the present accuracy, $B \rightarrow X_s \gamma$ already provides important constraints on the SUSY parameter space. With the start of the BABAR, Belle and CLEO III next year, the accuracy of the $B \rightarrow X_s \gamma$ branching fraction measurement will be significantly improved shortly. Sufficient B mesons will be produced in these experiments to make an observation of $B \rightarrow X_s l^+ l^-$ modes possible. Thus, em penguin decays may actually provide the first hints on physics beyond the SM.

Acknowledgments

I would like to acknowledge the CLEO collaboration for support with special thanks to T. Skwarnicki and E.H. Thorndike. I would also like to thank J.L. Hewett for sending me updated plots.

References

1. A.J. Buras *et al*, *Nucl. Phys. B* **424**, 374 (1998); A.Ali and C. Greub, *Z. Phys. C* **60**, 433 (1993).
2. K.G. Chetyrkin *et al*, *Phys. Lett. B* **400**, 206 (1997).
3. D.Boutigny *et al*, *SLAC Report* 504, 1056pp (1998).
4. A.J. Buras *et al*, *Phys. Lett. B* **414**, 157 (1997).
5. R. Ammar *et al*, *Phys. Rev. Lett.* **71**, 674 (1993).
6. M.S. Alam *et al*, *Phys. Rev. Lett.* **74**, 2885 (1995).
7. A.Ali and C. Greub, *Phys. Lett. B* **259**, 182 (1993).
8. T. Sjöstrand, *Comp.Phys.Commun.* 39, 347 (1986).
9. S. Glenn *et al*, preprint ICHEP98-1011, 11pp (1998).
10. R.Barate *et al*, *Phys. Lett. B* **429**, 169 (1998).
11. J.L. Hewett and J.D. Wells, *Phys. Rev. D* **55**, 5549 (1997).
12. M.N.Danielsen *et al*, proc. new dir. for HEP, Snowmass Co. (1996).
13. J.L. Hewett, private communication.
14. A. Ali and T. Mannel *et al*, *Phys. Lett. B* **264**, 505 (1991).
15. G. Buchalla *et al*, *Rev. Mod. Phys.* **68**, 1125 (1996).
16. S. Glenn *et al*, *Phys. Rev. Lett.* **80**, 2289 (1998).
17. R. Godang *et al*, preprint ICHEP98-1012, 18pp (1998).
18. C. Caso *et al*, *Eur. Phys. J. C* **3**, 1 (1998).
19. J. Alexander, plenary talk at ICHEP98, Vancouver, B.C., (1998).